ELSEVIER

Surface Science 347 (1996) 249–264

surface science

Hydrogen bonding on iron: correlation of adsorption and desorption states on Fe(100) and perturbation of the Fe–H bond with coadsorbed CO

Philip B. Merrill, Robert J. Madix *

Departments of Chemistry and Chemical Engineering, Stanford University, Stanford, CA 94305, USA

Received 7 October 1995; accepted for publication 2 October 1995

Abstract

Electron energy loss vibrational spectra suggest that hydrogen first adsorbs on Fe(100) in four-fold hollows (β_2) and converts to sites of lower ligancy (β_1) with increasing coverage. The β_1 state desorbs with pseudo first-order kinetics with an activation energy of 14.1 kcal/mol. The β_2 state exhibits a vibrational frequency of 700 cm^{-1}, indicative of adsorption in four-fold hollows. With increasing coverage this mode is replaced by a vibration at 1000 cm^{-1}, indicative of conversion of adsorbed H to an asymmetric position within the four-fold hollow. Adsorption of CO onto the H-covered surface causes an increase in the frequency of the mode near 1000 cm^{-1} associated with movement to a position of lower ligancy within the four-fold hollow.

Keywords: Adsorption kinetics; Carbon monoxide; Catalysis; Chemisorption; Electron energy loss spectroscopy; Hydrogen; Iron; Low index single crystal surfaces; Molecule–solid reactions; Thermal desorption; Thermal desorption spectroscopy; Vibrations of adsorbed molecules

1. Introduction

Because carbon monoxide facilitates hydrogen transfer reactions from Fe(100) to adsorbed alkyls [1,2], we have studied further the adsorbed state of hydrogen on Fe(100) and the effect of CO thereon. Previous work shows that simple alkenes adsorbed on a hydrogen-covered Fe(100) surface undergo hydrogen addition to form alkyl ligands upon heating, in competition with desorption of the alkene [3]. Further heating yields only the alkenes through a β-hydride elimination reaction, followed by the desorption of the hydrogen to leave the surface unchanged; no alkanes are formed. With coadsorbed CO, however, transfer of hydrogen from the surface to the alkyl group occurs upon heating to evolve the alkane into the gas phase at 170 K, a temperature lower than that observed for β-hydride elimination [1]. Temperature-programmed desorption (TPD) experiments with coadsorbed CO and H [4] suggest that CO induces the reaction by weakening the iron–hydrogen bond. In fact, this study demonstrates that this perturbation occurs immediately upon adsorption of CO onto hydrogen-saturated Fe(100) at 100 K, far below the temperature at which hydrogen transfer to adsorbed alkyls occurs.

The relationships between the state of CO adsorption and its desorption states on Fe(100)

* Corresponding author. Fax: +1 415 723 9780; E-mail: rjm@rio.stanford.edu.

SSDI 0039-6028(95)01016-5

has been studied extensively [4–9]. CO sequentially populates three adsorption states. Low exposures yield a single adsorption state (α_3) which demonstrates an unusually low CO stretching frequency of 1200 cm^{-1}. Upon heating, desorption of this CO(α_3) species at 410 K competes with dissociation to C_a and O_a, which in turn recombinatively desorb as CO(β) at 800 K. Saturation coverage of this adsorption state at 100 K is 0.58 ML [4]. The α_3 adsorption state represents CO in the four-fold hollows in a tilted binding configuration. Higher CO exposures allow further adsorption into bridge sites (α_2). The stretching frequency of this CO(α_2) species is 1900 cm^{-1}, and it desorbs at 300 K. Saturation CO exposures allow additional population of atop CO(α_1) with a stretching frequency of 2000 cm^{-1} which desorbs at 200 K.

Previous TPD [4] and EELS [9] experiments demonstrate that H_a strongly affects coadsorbed CO_a. On a hydrogen-presaturated surface, CO_a desorbs from strongly perturbed low temperature states below 350 K. Higher temperature desorption states appear unchanged, since hydrogen desorption is complete at 450 K. However, EELS demonstrates that adsorbed hydrogen blocks CO(α_3) adsorption (into four-fold hollows) on a hydrogen-presaturated Fe(100) surface at 100 K [9]; CO_a will not displace H_a at 100 K. Further, no phase separation of H_a and CO_a occurs upon coadsorption. Site conversion of CO from bridge and atop to four-fold sites occurs upon initial H_2 desorption from four-fold hollows. Desorption and dissociation of the CO(α_3) at 450 K proceeds from the four-fold hollows as observed on the clean surface.

CO markedly affects the TPD spectrum of hydrogen [4,10]. CO coadsorbed on the hydrogen-presaturated surface induces low temperature $H_2(\gamma)$ desorption states with peak temperatures between 170 and 250 K, compared to the $H_2(\beta_1)$ peak temperature from clean Fe(100) of 300 K. This effect has been interpreted as evidence for weakening of the iron–hydrogen bond [4]. Additionally, presence of the $H_2(\gamma)$ states correlates with the observed hydrogenation reactions of coadsorbed alkyls [1]. In contrast, when CO is preadsorbed before hydrogen exposure, CO merely blocks hydrogen adsorption. While CO will not displace H_a at 100 K, as previously noted, it is of interest that H_2 will not displace CO_a at 100 K either. Very little perturbation of the iron-hydrogen bond is observed with partial *pre*coverages of CO, as evidenced by the lack of $H_2(\gamma)$ desorption states; attenuation of the yield in $H_2(\beta_1)$ and $H_2(\beta_2)$ states appears to be the only significant effect of preadsorbed CO [4]. For this reason, the effects of preadsorbed CO will not be further discussed. We have verified all significant conclusions of the above studies in separate TPD and EELS experiments of hydrogen and CO on Fe(100) as lone adsorbates or upon coadsorption. Repetitious data has not been presented in this paper; however, minor deviations from the reported observations are noted in the results section.

Many complications commonly confront those attempting to observe metal hydrogen losses with EELS spectroscopy. A recent review summarizes these issues [11]. Small cross-sections for dipole scattering yield very weak losses; sometimes they cannot be observed. This difficulty may arise from small dynamic dipoles of the bonds due to similar electronegativities of H and the transition metal, or it may arise from relatively short M–H bond lengths which may allow the hydrogen to sit deep within the surface, so as to be almost completely electrically screened. Electronic excitations of the metal are possible which, if modified by adsorbed hydrogen, can create confusion. Several authors have reported maxima and minima in the electron reflectivity as a function of primary energy due to surface resonances [12–15]. In these same systems, the cross-section of M–H vibrational excitations show maxima as a function of E_p which correlate with minima in the reflectivity curve. The result of such phenomena can make the observation of a M–H vibration quite elusive, particularly if the spectrometer is tuned to maximize intensity of elastically scattered electrons, as is common.

Our previous EELS results of coadsorbed H_2 and CO demonstrate only the influence of H_a upon CO_a. New TPRS and EELS studies, presented here, are intended to emphasize the adsorption states of hydrogen and the influence of CO thereon; they represent the first vibrational observation of hydrogen on the clean Fe(100) surface or in the presence of coadsorbed CO.

2. Experimental

Experiments were performed in a stainless steel ultra-high vacuum chamber with a base pressure of 3×10^{-11} Torr capable of low-energy electron diffraction (LEED), Auger electron spectroscopy (AES), temperature-programmed reaction spectroscopy (TPRS) and high-resolution electron energy-loss spectroscopy (HREELS) measurements. The temperature of the Fe(100) crystal, mounted on a rotatable manipulator with three degrees of freedom, could be controlled from 100 to over 1000 K. The sample was cooled by thermal conduction from a liquid nitrogen reservoir. Heating was done resistively with current flow through the tantalum support. Linear heating rates of 5–6 K s^{-1} were used for TPD experiments. Temperature was monitored with a chromel–alumel thermocouple spot-welded to the crystal. The UTI-100C quadrupole mass spectrometer was computer-driven to allow collection of up to 10 masses concurrently. For example, with scan times of 25 ms for each mass to be monitored, a complete scan of 10 masses with a heating rate of 4 K s^{-1} could be accomplished with a temperature resolution of 1 K. The ionization cage of the mass spectrometer was enclosed by a glass cap with a collimating orifice approximately 5 mm in diameter in order to limit analysis to products desorbing in line of sight from the area of the crystal positioned directly in front of the cap opening. HREELS was conducted with a double-pass 127° cylindrical sector monochrometer and a single-pass analyzer. The typical full width at half maximum (FWHM) for elastically scattered electrons was about 70 cm^{-1} but ranged from 60 to 100 cm^{-1}. These resolutions were utilized to enhance the relatively weak M–H losses, which never exceeded 40 Hz. The gases were used as supplied from Matheson without further purification; they included argon (prepurified, 99.998% min.), ethylene (C.P., 99.5% min.), hydrogen (prepurified, 99.99% min.), deuterium (C.P., 99.7% min.) and carbon monoxide (research grade, 99.99% min.). Two capillary array dosers were utilized so that contamination of one gas by another would not occur. CO was dosed indirectly from the background at a pressure of 2×10^{-9} Torr to allow reproducible exposures. The exposures for CO are expressed in Langmuirs (10^{-6} Torr·s). Dosing of hydrogen, deuterium and ethylene was directed from capillary array dosers at close distances; the saturation exposures were easily reproduced, and chamber pressures were kept to a minimum. The hydrogen and deuterium exposures stated in this work assume a doser enhancement factor of 10 with direct exposure versus background exposure. Poor sticking probabilities of H_2 and D_2 required 600 L exposures to saturate the Fe(100) crystal.

Details of the preparation and initial cleaning of the Fe(100) crystal are given elsewhere [4]. Routine cleaning was accomplished with Ar ion bombardment. First the crystal was heated to 923 K and sputtered for 10 min; the crystal was then allowed to cool to 105 K before sputtering for another 10 min. Following evacuation to 10^{-10} Torr, the crystal was then annealed at 723 K for 5 min. AES and EELS were used to evaluate surface cleanliness. A $c(2 \times 2)$ random $C_a + O_a$ overlayer resulting from the dissociation of CO_a [16] was used for AES calibration; XPS studies report dissociation of 0.24 ML of CO yield this state [17]. This cleaning procedure very efficiently eliminated surface carbon (0.00–0.01 ML by AES) (none detected by EELS), but was not always completely successful in removing oxygen as indicated by M–O losses [18] detected by EELS. Prolonged heating above 727 K will bring dissolved oxygen from the Fe(100) bulk to the surface if any exists [18]. Excessive oxygen impurities were removed with ethylene titrations, as was necessary after exposure of the crystal to atmospheric pressures for routine maintenance or in cases where very large quantities of O_a accumulated on the surface and the routine sputtering procedure yielded little progress. However residual carbon, a product of the reaction, then needed to be sputtered away. For minor oxygen impurities, O_a could be titrated off at the expense of C_a. When minor levels of impurities persisted, TPRS experiments were performed to ensure that these impurities had no measurable effect on the CO-induced hydrogen transfer reaction to the alkyl groups. Upon heating, atomic oxygen reacted with ethylene to form combustion products leaving behind

residual carbon, but most of the ethylene cleanly desorbed in the manner expected for an impurity-free hydrogen-presaturated surface [3]. With these procedures, the O_a impurities could be greatly reduced (0.01–0.03 ML by AES). EELS of the surface, however, demonstrated remarkable sensitivity to these quantities of oxygen. While the impurity could be controlled to a level where reactivity was not affected, the M–O losses were observed in many cases when detecting the weak M–H losses.

The TPD and EELS data presented has been smoothed with a standard nine-point averaging algorithm. Care was taken to assure that the peak shapes of the smoothed data represent both the peak heights and widths of the raw data. Temperature-programmed desorption collection parameters were chosen to allow as much data as

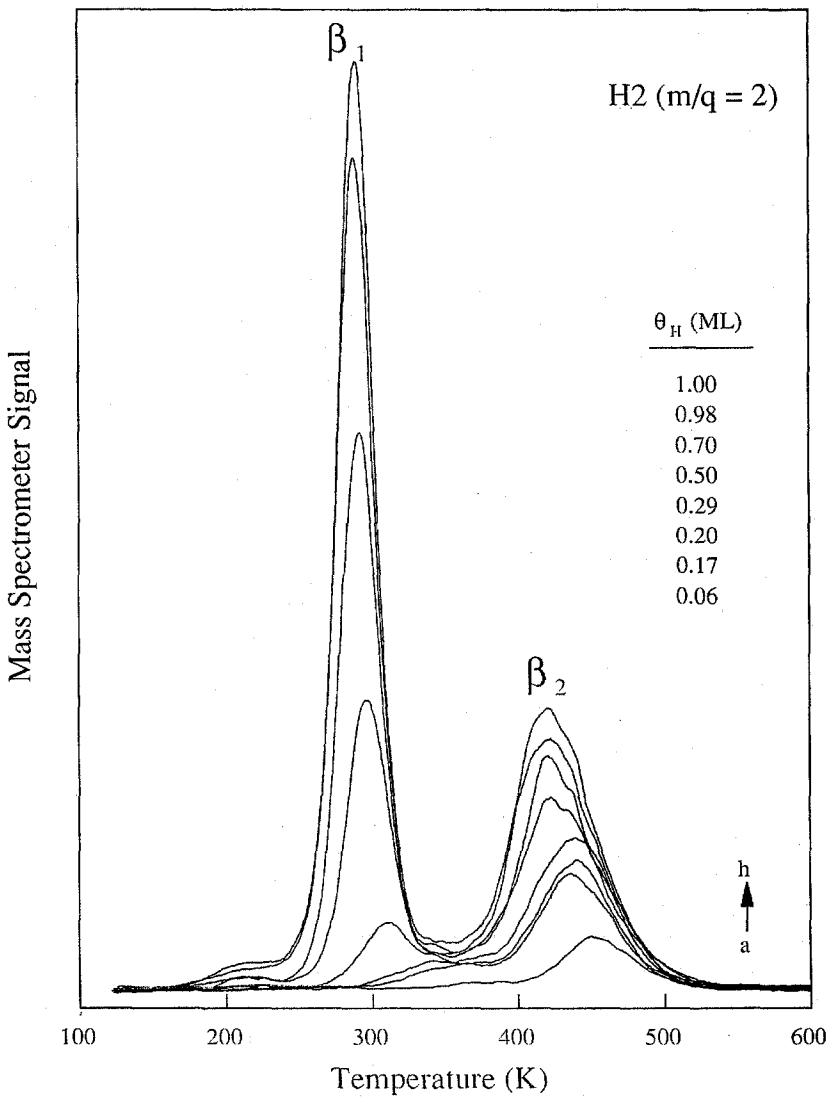

Fig. 1. Hydrogen thermal desorption from Fe(100) as a function of increasing H_2 exposure. Heating rates are 6 K s^{-1}.

possible to be available for kinetic analysis. Signal-to-noise ratios for the same experimental parameters were better in the case of deuterium than hydrogen due to smaller background levels.

Experiments were performed for a large range of CO coverages (0.07–0.58 ML) on hydrogen pre-exposed surfaces of varying coverage (0.7–1.0 ML). For H_2, TPD desorption traces could be collected one after another with no cleaning necessary. Exposures were not done exclusively in increasing or decreasing order. However, collection of a single EELS spectrum took over an hour, requiring periodic cleaning of the surface. Where possible, the initial surface was prepared, a spectrum was collected, the crystal was removed from the spectrometer for additional dosing, and then repositioned in the spectrometer for further analysis. Successive doses were examined until the surface showed signs of contamination from background adsorption, such as O–H losses near 1300 cm^{-1} from water adsorption [19] or carbonyl stretches at 1200 or 2000 cm^{-1} from coadsorbed CO [7–9].

3. Results

3.1. Hydrogen on Fe(100): temperature programmed desorption (TPD)

The population of desorption states as a function of coverage or exposure is similar for both H_2 and D_2 (Figs. 1 and 2). Low exposures yield a single desorption state at 450 K (β_2). Higher exposures produce desorption from an additional state at 300 K (β_1). In contrast to results reported previously [4], in these studies the β_2 state did not saturate before population of β_1 began. Additionally, the peak temperature of β_2 appears to be 25 K higher at the largest exposures than previously reported. The saturation coverage was previously determined to be 1.0 ML [4]. Coverages were determined by ratioing the integrated areas under each TPD trace to that at saturation.

The activation energy for desorption for the β_1 state was determined with an isotherm–isostere analysis [20]. Burke and Madix [4] determined the E_a and ν by heating rate variation [21] to be 17 kcal/mol and 3×10^{12} s^{-1} for the H-saturated Fe(100) surface, but did not consider partial coverages. An isotherm–isostere analysis was applied to TPD traces for the β_1 state for $\theta_H \geq 0.25$ ML. For H_a, the activation energy was calculated to be 14.1 ± 0.3 kcal/mol with an *apparent* reaction order of 1.4 ± 0.1. Analysis of the D_a data yielded an E_a of 14.6 ± 0.2 kcal/mol and an *apparent* reaction order of 1.4 ± 0.1 [22]. The near constancy of the peak temperature of the β_1 state with coverage suggests the reaction order for desorption is one near saturation, but the kinetics are coverage dependent and not simple. The isosteres were nearly parallel and thus indicate that after initial population of the β_1 desorption state, the activation energy for desorption does not appear to significantly differ from that of the saturated layer. No further studies were performed to clarify these details.

No kinetic isotope effect was observed for desorption from the β_1 state. From the isotherm–isostere analysis, differences between the desorption activation energies for the isotopes, as determined by the above analysis, did not deviate significantly from experimental error. Fig. 3 shows a composite TPD for a few coverages of H_2 and D_2. If their were a normal isotope effect, we would expect a significant shift to higher temperature for the spectra of the heavier isotope.

3.2. Hydrogen on Fe(100): electron energy loss spectroscopy (EELS)

The electron energy loss vibrational spectra show the evolution of two features as the hydrogen coverage is increased (Fig. 4). The energy loss at 400 cm^{-1} due to the impurity of O_a does not obscure the rest of the spectrum, nor does its presence alter the observed H_a losses, as confirmed by separate spectra without O_a at isolated hydrogen coverages. In particular, the presence of two distinct losses is not an effect of the oxygen, and the frequencies do not appear to be altered by the presence of oxygen. The loss represents an impurity of less than 0.03 ML O_a, as determined by AES. O_a impurities of this level do not create an observable effect upon the CO-promoted

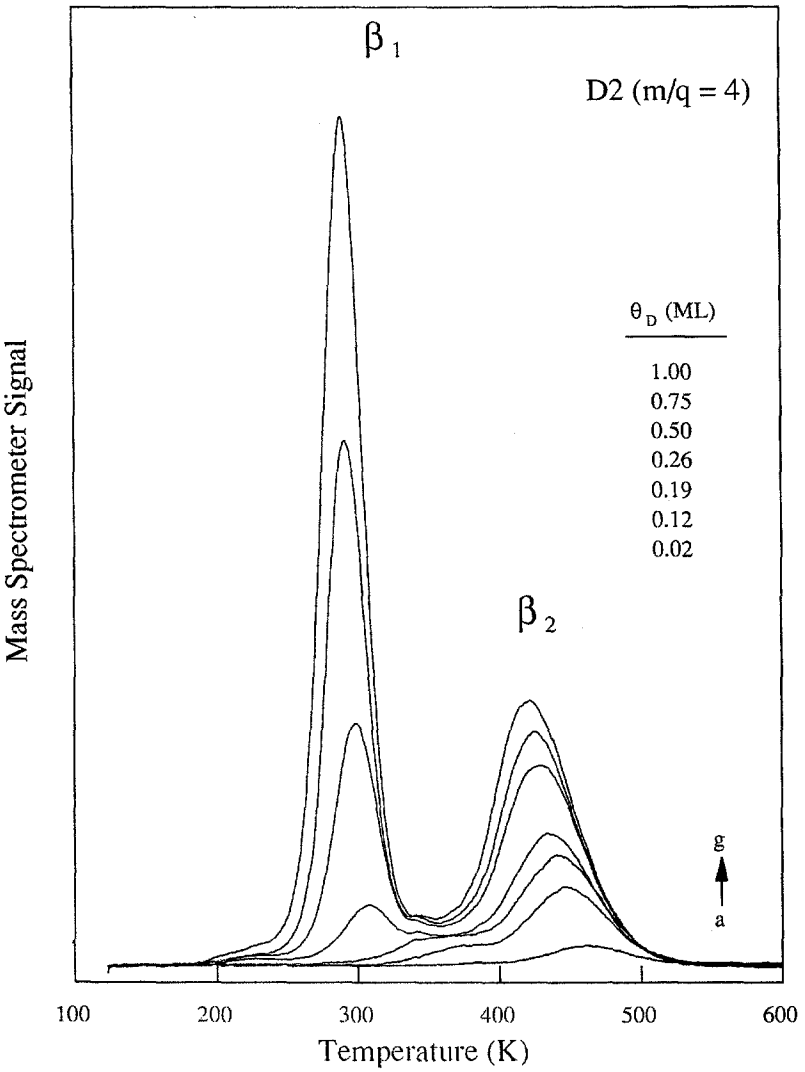

Fig. 2. Deuterium thermal desorption from Fe(100) as a function of increasing D_2 exposure. Heating rates are 6 K s^{-1}.

hydrogen transfer reaction to surface alkyl groups. We thus conclude that the observed O_a impurity has no observable effect on the adsorbed hydrogen.

The evolution of the EELS features parallels the occupation of the β_1 and β_2 states. Low hydrogen coverages demonstrate a low frequency loss at 700 cm^{-1}, which correlates with the high temperature β_2 desorption feature. Higher hydrogen coverages show the appearance of an additional high frequency loss at 1000 cm^{-1} which correlates with the low temperature β_1 desorption feature, which dominates at saturation coverage. The high frequency loss is only observed at coverages which would also lead to β_1 desorption. Vibrational spectra of deuterium on Fe(100) show a correlation of the $D_2(\beta_1)$ with a loss at 750 cm^{-1}, corresponding to an isotopic shift, ν_H/ν_D, of 1.33 from the $H_2(\beta_1)$ loss, as is expected for a stretching frequency of the isotopes [23]. A lower frequency loss, to correlate to the $D_2(\beta_2)$, was not observed or resolved from the β_1 loss or elastic peak.

Over a 3.5-eV range the loss intensities for

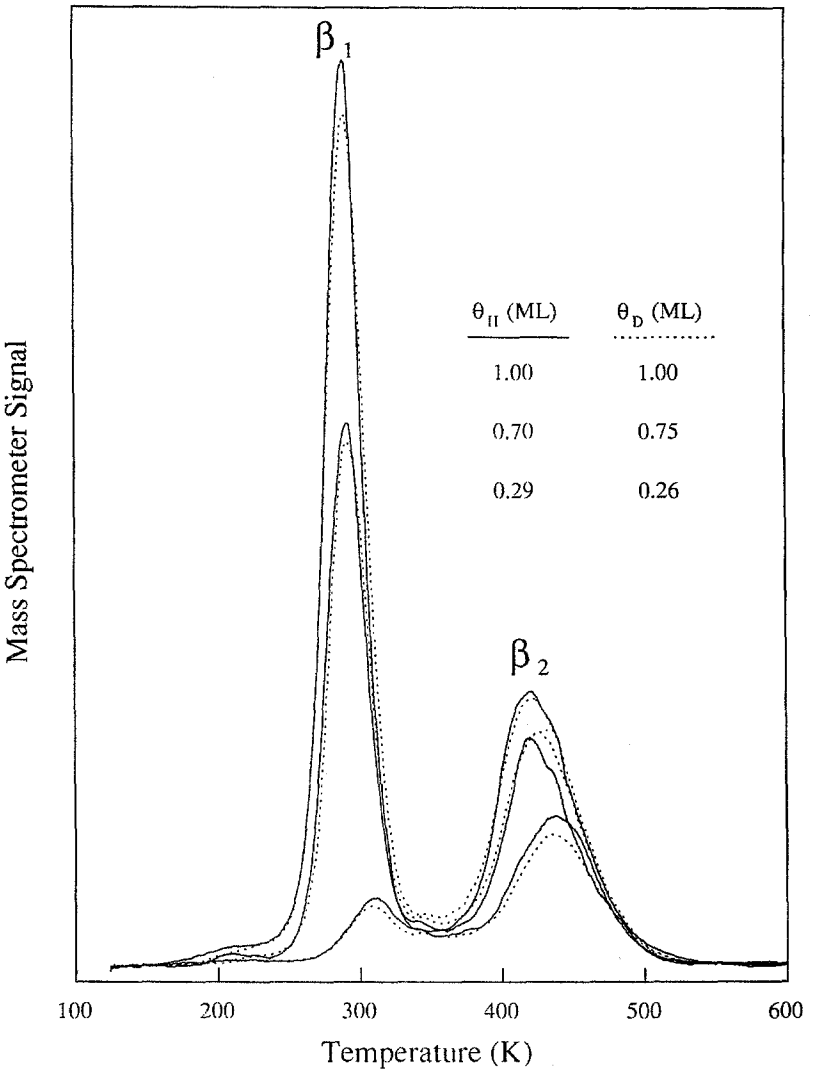

Fig. 3. Thermal desorption–isotope overlays. Curves were selected for hydrogen (Fig. 1) and deuterium (Fig. 2) of similar coverage to demonstrate the lack of an observable isotope effect. A noticeable shift to higher temperature would be expected for the heavier isotope in the event of tunneling assisted desorption.

adsorbed hydrogen demonstrated differing dependencies upon the primary electron energy. Within this range, the loss intensity of the high frequency feature remained relatively constant. However, the ratio of intensities of the low frequency loss to the high frequency loss ranged from nearly zero to one. For this reason, care was taken throughout this work to use the same primary energy in obtaining all spectra. For a given primary energy, the comparison of the intensities of the β_1 and β_2 loss is meaningful, and relates to the relative quantity of the species. However, for significantly different primary energies, the intensity changes of β_1 and β_2 cannot be easily related to coverage changes. For this reason, sample biases were also fixed, rather than adjusted to maximize elastic signal at the onset of tuning, in order to prevent changes in the primary energy.

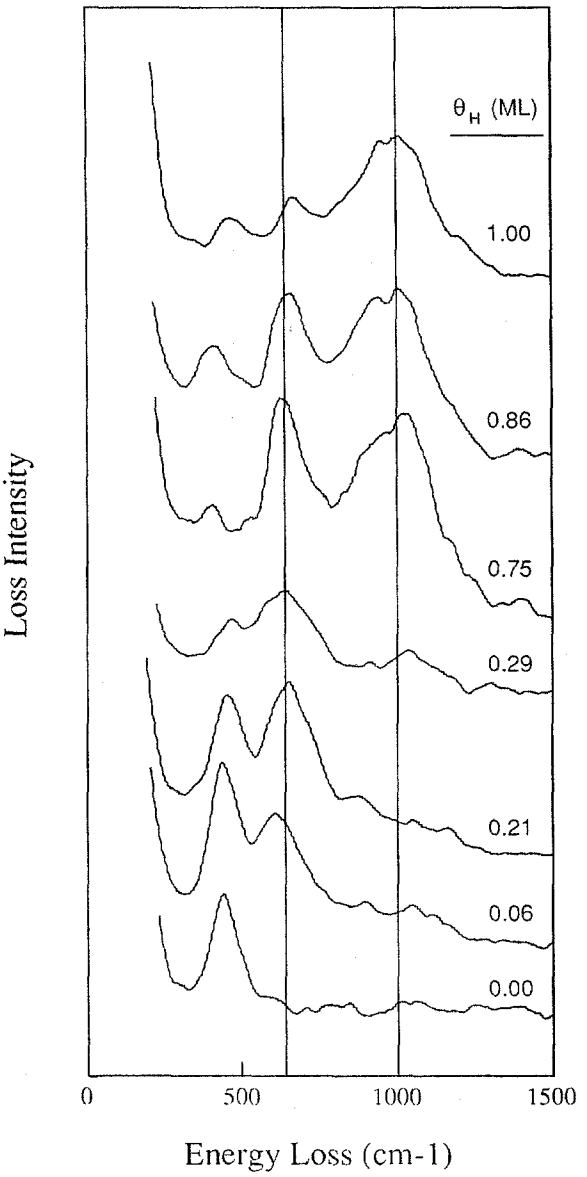

Fig. 4. EELS of H adsorbed on Fe(100) as a function of increasing H coverage, as in Fig. 1. The temperature of adsorption was 100 K.

3.3. *Coadsorption of hydrogen and carbon monoxide on Fe(100): the influence of post-dosed CO_a upon H_a*

Vibrational spectra of the hydrogen adlayer at 110 K reveal a perturbation of the iron–hydrogen bond by postdosed CO (Fig. 5). These effects were reproducible. In this figure the $H_2(\beta_2)$ and $H_2(\beta_1)$ losses for a total coverage of 0.86 ML are clearly visible at 700 and 1000 cm^{-1} without the coadsorbed CO (spectrum b). Upon initial exposure, CO adsorbs into four-fold hollows (1200 cm^{-1}) as well as bridge and atop sites (near 2000 cm^{-1}) on the non-saturated hydrogen adlayer (spectrum c). Further adsorption of CO shows additional population of the 2000-cm^{-1} feature as the four-fold sites become saturated. A strong M–CO stretching loss near 450 cm^{-1} accompanies the coadsorption of CO. The high frequency $H_2(\beta_1)$ loss near 1000 cm^{-1} is observed to shift to higher energy with increasing CO coverage.

Several precoverages of hydrogen were studied; this shift to higher frequency is observed for all precoverages of hydrogen. Fig. 5 best demonstrates the shift with the 1200-cm^{-1} $CO(\alpha_3)$ loss as a benchmark. The results are summarized in Fig. 6. Though slight differences exist for various precoverages due to difficulties in clearly defining the peak energy for the broad peaks, the trend is clear. The magnitude of the shift appears to be as great as 150–200 cm^{-1}, but at the highest values the frequencies were difficult to determine accurately due to interference from the $CO(\alpha_3)$ loss.

Substantial differences in screening of the hydrogen losses by coadsorbed CO is observed. The intensity of the loss at 1000 cm^{-1} is greatly attenuated with sequential exposures of CO, while at the same time undergoing a shift to higher frequency. Adsorption of CO molecules in the bridge and atop positions may electrostatically shield the low lying hydrogen atoms. However, with attention to beam energies to assure observation of the low frequency loss near 700 cm^{-1}, no attenuation of the low frequency mode is observed. Rather, with coadsorption of CO, the M–CO stretch eventually overwhelms the low frequency loss. The differences in screening may indicate that the two modes are due to hydrogen atoms of different local environments.

A minor loss was observed here at 1600 cm^{-1} on both the clean and hydrogen-covered surfaces. Fig. 5 (spectrum d) demonstrates the intensity saturates with low CO coverage. This loss has previously been reported on the Fe(100) surface by

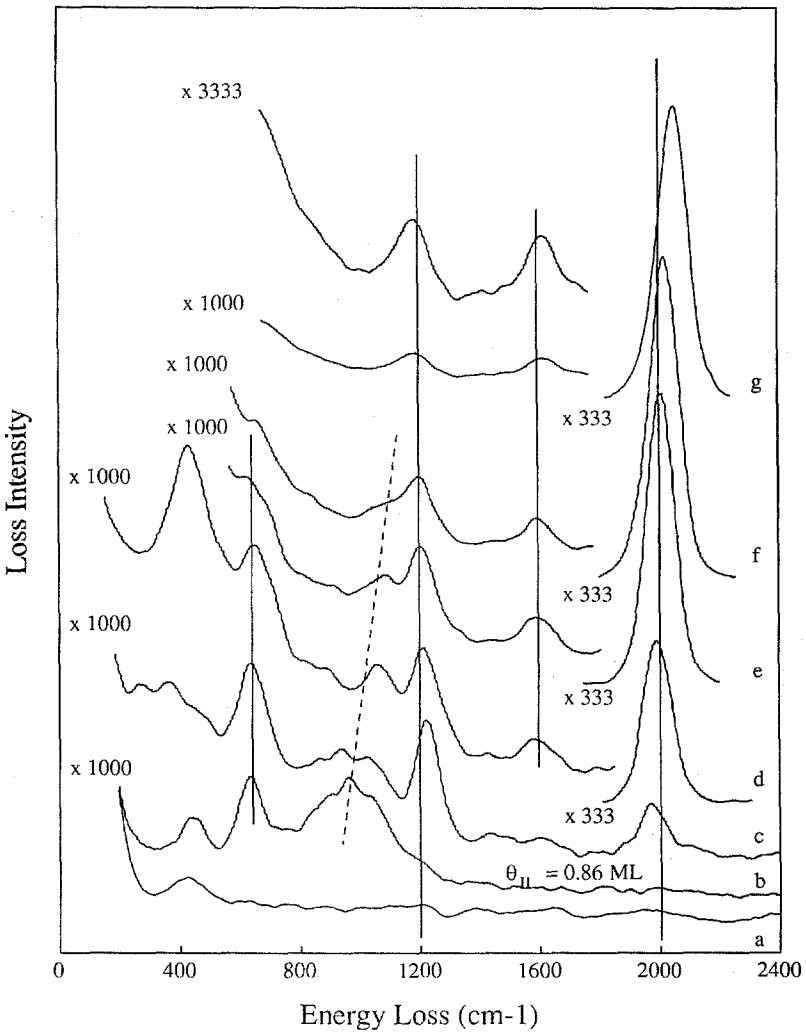

Fig. 5. EELS of CO and H coadsorbed on Fe(100): (a) Fe(100) surface with 0.03 ML oxygen impurity; (b) initial θ_H=0.86 ML; (c–g) +increments of CO at exposures of 0.125, 0.25, 0.375, 0.5 and 1 L. The shift of $\beta_1\nu_{M-H}$ is clearly seen with increasing CO coverage. CO was adsorbed on the hydrogen adlayer at 100 K.

Benndorf et al. [8]; they attributed the loss to CO adsorbed at step sites of the Fe(100) crystal [24]. Initially, we observed no 1600-cm^{-1} loss on the clean or hydrogen-presaturated Fe(100) surface [9] as was the case with Moon et al. [7] on the clean surface. However, with repeated experiments, this state became noticeable. At saturation exposures, the loss amounted to less than 1% of the area of the 2000-cm^{-1} loss. The appearance of this mode was not accompanied by any effect on the TPRS, EELS or surface reactivity for alkyl hydrogenation.

4. Discussion

4.1. Hydrogen species at low and high coverages

Three possibilities were considered to explain the EELS and TPD of the hydrogen overlayer:

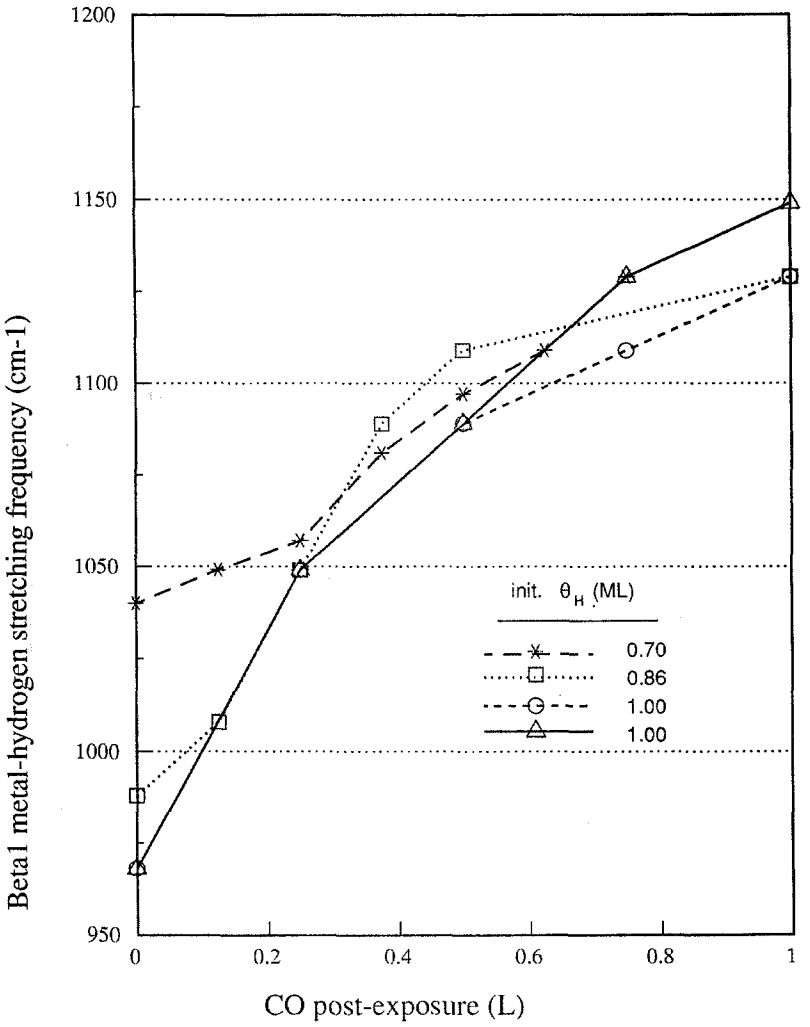

Fig. 6. Metal–hydrogen stretch versus CO coverage. The plot summarizes results from several experiments with different initial hydrogen precoverages. All exhibit the shift to higher frequency.

(1) two distinct species coexist above $\theta_H = 0.75$, each possessing different local geometries; (2) a species present at low coverage converts to another at higher coverage; (3) a single species exists which possesses the same local geometry at all coverages.

The existence of a single hydrogen species throughout the entire coverage range on Fe(100) is inconsistent with the data. Certainly, evolution of multiple temperature-programmed desorption states in recombinative desorption with increasing coverage may occur as next nearest neighbor sites are occupied at coverages above half a monolayer. In such a case the binding site symmetry and coordination are the same, but the desorption energetics change due to the lower differential energy of adsorption at the higher coverage. An example of such a case is nitrogen desorption from W(100), for which two desorption states evolve sequentially with increasing coverage [25]. In this case, however, the vibrational frequency of the adsorbed nitrogen atoms shifts from 525 to 274 cm^{-1} as the binding energy decreases [26], in contrast to the behavior observed here. Generally, for such a case it is expected that the vibrational

spectrum would convert smoothly from one loss at a high frequency to another at a lower frequency as the surface coverage increases. Another relevant example is H on W(100), for which a phase transition occurs with increasing H coverage giving rise to two desorption features much like those observed here. However, in that case the vibrational spectrum is characteristic of a single bridging species over the entire coverage range, accompanied by a continuous shift in loss energy [16,27–29].

Also of note is that the high (β_1) and low (β_2) frequency losses do not fill in simultaneously as would be expected for a single adsorbate possessing a symmetry which allowed two observable modes. A pathological condition, in which one of two vibrational modes allowed for a single site symmetry becomes observable only as coverage increases is, however, consistent with the observations. A reasonable source of such behavior is the dependence of the loss intensity of one mode on beam energy which may vary slightly with coverage due to a change in the work function. Indeed, we do observe that the presence of the loss at lower energy depends on electron beam energy.

Though we have not studied the energy dependence in detail, we believe that this effect does not account for the appearance of the lower energy loss with increasing coverage. In this case, appreciable variations in intensity occurred only over a 3.5-eV change in primary energy. We are aware of only one report which demonstrates for a single adsorbed species a difference in the sensitivities of two modes upon the primary energy [30]. Over a range of 3 eV, the maximum intensity of one loss diminished to zero while others approached a maximum. For H on Fe(100) the work function changes less than 0.1 eV between 0.25 and 1.0 ML [31]. These changes are too small to account for the gradual appearance of the loss at 700 cm^{-1}. More importantly, the high frequency loss, which is absent at low coverages, appears insensitive to primary energy over the range studied; thus, its absence cannot be due to such an effect.

The data suggest that a single species dominates at low coverage, but another species dominates at high coverage. The most reasonable explanation of the observations is that two species coexist at the higher coverages, one of which also exists in the lower coverage regime.

The species existent at high coverage possesses both a lower activation energy for desorption and a higher vibrational frequency. At saturation coverage the low desorption energy–high frequency state appears to dominate [32].

4.2. Site assignment of $H_2(\beta_1)$

All existing evidence suggests that adsorbed hydrogen atoms occupy the four-fold hollow sites at saturation coverage. The most direct evidence is that adsorbed hydrogen blocks CO(α_3), which is known to occupy the four-fold hollow [17,33,34]. Furthermore, the saturation coverage of 1.0 ML [4] suggests either four-fold or atop binding sites. Atop sites are not expected to be favorable binding sites due to the higher ligancy of bridge and four-fold sites. Terminally bound hydrogen on single crystals is limited to semiconductor surfaces, where covalent bonds best describe the species [11]. Furthermore, on W(100), where hydrogen occupies two-fold bridge positions, the saturation coverage is 2.0 ML, twice that on Fe(100).

The exact position of hydrogen within the four-fold hollow is not known. MINDO calculations [35] simulating adsorption of hydrogen on Fe(100) with an $Fe_{12}H$ cluster indicate the most stable binding site is off center in the four-fold hollow with three-fold coordination. It is reasonable to expect CO adsorption in the hollow to be blocked if hydrogen occupies this asymmetric site. The binding energy of the hydrogen atom was calculated as it was moved from the bridge center site to the four-fold center while at an equilibrium distance from the surface at each step. The calculated binding energies were 60 kcal/mol at the bridge center, 56.7 kcal/mol at the hollow center, and 60.7 kcal/mol in between at a pseudo three-fold binding site. Additional features of this calculation demonstrate an inverse relationship between the ligancy and the perpendicular M–H stretching frequency for the four-fold (1151 cm^{-1}), bridge (1343 cm^{-1}) and atop (1953 cm^{-1}) sites. Given that 1000 cm^{-1} is characteristic of hydrogen in the

four-fold hollow, the frequency observed here for the β_1 state clearly indicates high ligancy [11,36].

Fig. 7 shows hydrogen bound in either the bridge center, asymmetric three-fold or four-fold centered sites of the hollow on the Fe(100) surface. The positions of hydrogen for these representations were taken from the aforementioned $Fe_{12}H$ cluster calculations [35] where the Fe–H distances were calculated. This representation shows that indeed it is reasonable to assume that the hydrogen atom may access several bonding geometries within the four-fold hollow. In fact, a continuum of bonding geometries exists between the four-fold hollow center and bridge center. The $Fe_{12}H$ cluster calculations with hydrogen centered in the hollow yielded nearly equivalent diatomic energies (and bond orders) of the hydrogen with the five nearest iron atoms [35]. This represents a ligancy of five. At the bridge center, bond orders and diatomic energies of hydrogen in the 12-metal atom cluster indicate a ligancy of two. Bond order information was not provided for the asymmetric binding within the hollow, but a ligancy of three seems reasonable. This provides a decrease in ligancy from the center of the hollow to the asymmetric three-fold site and then to the bridge center site. We expect movement of the hydrogen from the asymmetric position towards the center of the hollow would decrease the frequency of the Fe–H stretch; while movement away from the center would increase the frequency, as we observe.

In general, vibrational frequencies of H on metals decrease with increasing ligancy for vibrational motion perpendicular to the surface [36]. Terminal bonding (ligancy of one) on single crystals yielded very high frequencies (1980 to 2100 cm^{-1}); they are thus far observed only on semiconductor surfaces such as silicon, gallium arsenide, germanium, indium, etc. [11]. Vibrational frequencies do not differ significantly enough for sites with ligancy of two or three to differentiate these solely upon their values. However, these frequencies tend to be larger than for adsorption involving ligancy of four. Hydrogen on W(100) [29] occupies a bridge site with perpendicular frequency ranging from 1250 to 1010 cm^{-1} with increasing coverage [16,28]. A bending mode exists at 640 cm^{-1} and is observable off-specular. An asymmetric or paral-

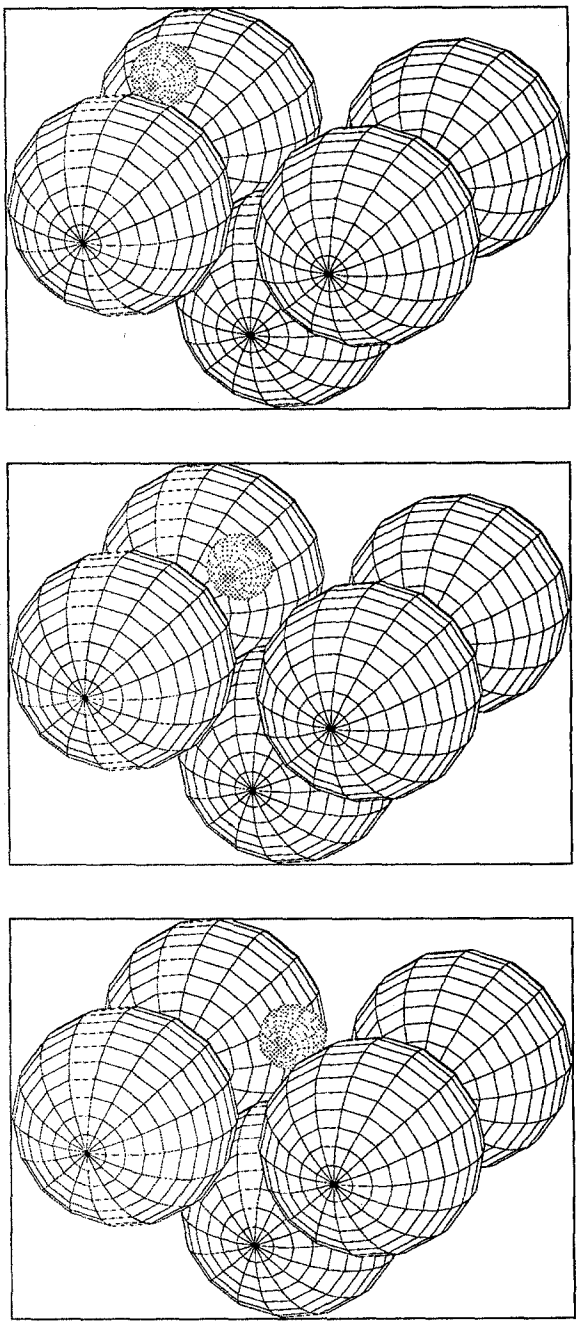

Fig. 7. Conceptual pictures: hydrogen bound on the Fe(100) hollow at the (top) bridge center, (middle) asymmetric three-fold hollow and (bottom) center of four-fold hollow. Covalent radii are shown for Fe atoms (1.24 Å) and H atom (0.37 Å) [64]. Distances are equilibrium values as calculated for an $Fe_{12}H$ cluster, after Blyholder et al. [35].

lel mode (overtone of ν_w) is observable off-specular which ranges from 970 to 1290 cm^{-1} with increasing coverage. Bridge bonding has also been observed for hydrogen on W(110) [37,38] and Mo(100) [39,40]. On Ni(111) [41], Pd(111) [14], Ru(0001) [13,42], Rh(111) [30,43] and Pt(111) [12] hydrogen adsorbs symmetrically in the three-fold hollows. The general vibrational features are one dipole active mode (500–850 cm^{-1}) and one impact scattered mode (950–1250 cm^{-1}). The Fe(110) surface shows hydrogen losses at 1060 cm^{-1} (specular) and 880 cm^{-1} (off-specular) [44]. Based upon a single dipole mode, it was concluded that the features represented symmetric and asymmetric stretches of a two-fold bound species across the short bridge. More recent low energy electron diffraction studies assert a three-fold species and point to a possible misinterpretation of the vibrational data [45]. An *R*-factor analysis of the *I/V* curves rule out atop and short bridge sites; the *R* factors significantly favor the assignment to the three-fold site rather than the long bridge. "Quasi" three-fold hollow species have been proposed for Ni(110) [46–50], Rh(110) [51] and Ru(10$\bar{1}$0) [52]. A principle dipole active mode (650–800 cm^{-1}) along with two non-degenerate parallel modes (800–1300 cm^{-1}) are reported for these surfaces. The symmetric four-fold hollow (C_{4v}) binding site is reported for Ni(100) [53,54], Rh(100) [55] and Pd(100) [56,57] with a single dipole active mode at about 500–700 cm^{-1}.

For the H/Fe(100) system, the relevant literature would suggest that a ligancy of two or three is most consistent with the 1000-cm^{-1} loss, because this frequency is high for a hydrogen bound with a ligancy of four. Symmetry arguments based upon the number of modes observed in the specular or off-specular directions do not help with the H/Fe(100) system. Count rates were so low that off-specular data was of no use. Additionally, as was the case with Rh(111) [43], allowed modes may not be observed with an adsorbate such as hydrogen with its many complications. Combined with the fact that $H_2(\beta_1)$ blocks CO adsorption in the four-fold hollow, we assign the binding site of $H_2(\beta_1)$ to pseudo three-fold sites within the four-fold hollow on Fe(100).

4.3. Site assignment of $H_2(\beta_2)$

Since the high (β_1) frequency loss grows in at the expense of the low (β_2) frequency loss, it appears that the β_2 state is converted to the β_1 state as coverage is increased. At saturation coverage the β_1 state dominates. In addition, the TPD show in these studies that, at saturation coverage, 40% of the hydrogen desorbs through the β_2 state. The high coverage in the β_2 desorption state suggests that desorption from this state is *not* associated with surface defects. We take the single, intense vibrational loss feature at 700 cm^{-1} exhibited by the β_2 state to be indicative of motion perpendicular to the surface by atoms bonded in the center of four-fold hollows, in accord with assignments on other surfaces. The conversion of hydrogen from a ligancy of four to three that appears to occur may be accompanied by structural rearrangement of iron atoms at the surface, but we have no other evidence to corroborate this. The independent kinetic parameters of desorption before and after such a phase transition could easily differ to yield unique desorption states; hydrogen desorbing from Mo(100) experiences several phase transitions which demonstrate this behavior [58]. In that system, hydrogen resides in bridge positions through many phases, while the underlying structure of Mo chains change, yielding unique desorption parameters for each phase.

The TPD results indicate that the higher frequency species (β_1) desorbs at lower temperature, implying a lower binding energy and a lower Fe–H bond strength. However, the frequency for motion perpendicular to the surface is not a good measure of the metal–hydrogen bond strength [36]. Indeed, for atoms adsorbed on metals, the frequency of the mode perpendicular to the plane of the atoms to which it is immediately bound decreases with increasing ligancy *for identical binding energies to the surface.* Mate et al. [30] considered heats of adsorption and M–H vibrational frequencies for hydrogen systems where both have been reported; it seems clear that the frequency is more sensitive to the coordination number of the adsorbed H than to the M–H bond strength. If the binding geometries were different, higher ligancy could significantly lower the stretching frequency of the

β_2 species, while at the same time represent a higher binding energy.

Consequently, it appears that atoms adsorbed in four-fold hollows at lower coverage desorb with approximately second-order kinetics and an activation energy of 23 kcal/mol [4], whereas those atoms adsorbed in the three-fold coordination sites desorb with pseudo first-order kinetics and an activation energy of 14.1 kcal/mol. The desorption energy of the β_2 state is nearly the same as that observed for hydrogen desorption from Ni(100) [59–61], Ni(111) [60,62] and Pd(100) [63] for which second-order kinetics have been documented. The lower value of the desorption energy at high coverages and the pseudo first-order behavior is suggestive of the formation of islands of three-fold coordinated hydrogen in which neighboring hydrogen atoms are geometrically predisposed to recombine. The relaxation of iron atoms into energetically more favorable positions during desorption may contribute to the lowered desorption energy. Again, the H/Mo(100) system demonstrates such an effect where the hydrogen coverage-dependent phase transitions are well documented [58].

4.4. *Influence of CO_a upon H_a: perturbation of the iron-hydrogen bond*

Coadsorbed CO clearly perturbs the iron-hydrogen bond, as evidenced by both the TPD and EELS experiments; both low temperature hydrogen desorption states and a shift of iron–hydrogen stretching frequency with coadsorbed CO are observed. We propose that CO_a promotes a binding geometry change of hydrogen within the four-fold hollow.

The frequency shift cannot represent Fe–H bond strengthening. Low temperature $H_2(\gamma)$ desorption states in the TPD experiments clearly indicate that the Fe–H bond is weakened by the coadsorbed CO. EELS also shows that desorption of H_2 from the γ-states leads to CO conversion from bridge and atop to four-fold hollows. This demonstrates that the $H_2(\gamma)$ desorption states are associated with the four-fold hollows. Thus the CO is inducing a frequency shift of the hydrogen within the hollows which is not indicative of an increase in bond strength.

The frequency shift is thus attributed to a site or geometry change of the hydrogen binding within the four-fold hollow. As noted in the above discussion of hydrogen on clean transition metals, stretching frequencies are extremely sensitive to binding geometry. Further, the ability of hydrogen to block the hollow site for $CO(\alpha_3)$ adsorption need not be affected by movement of hydrogen to an asymmetric position within the hollow, since the side-on bonding of CO must involve several iron atoms within the four-fold hollow. We suggest that the observed shift of the $\beta_1 \nu_{M-H}$ loss to higher energy and weakened M–H bond with increased coverage of coadsorbed CO represents the movement of hydrogen from the asymmetric three-fold site of the hollow, further towards the two-fold bridge position.

4.5. *CO-promoted hydrogen transfer reactions*

The behavior of coadsorbed CO_a and H_a as observed in this work contributes to our understanding of CO-promoted hydrogenation of surface alkyl groups. Modification of the iron–hydrogen bond has been clearly demonstrated even at temperatures far below the reaction conditions. The role of CO cannot be as simple as moving into the vacated hydrogen site in a concerted fashion as the reaction proceeds. However, the ability to do so along with the strong bonding of the "lying down" species may contribute to reducing the enthalpy of the overall reaction. The coadsorbed CO_a weakens the Fe–H bond and "pushes" the hydrogen further away from the center of the hollow. When surface alkyl groups are coadsorbed with the H_a and CO_a, hydrogen transfer to form gas phase alkanes occurs upon heating. Without the CO_a the hydrogen transfer is not facilitated; rather the alkyl groups remain until β-hydride elimination removes them from the surface as ethylene. It is important to emphasize however, that the perturbation of the Fe–H bond occurs upon the coadsorption of CO_a and H_a with or without surface alkyl groups, even at low temperatures.

5. Summary

Vibrational spectroscopy has been utilized to investigate the adsorption of hydrogen on Fe(100) and the perturbation of the Fe–H bond by coadsorbed CO. A correlation has been made between the vibrational features of the adsorbed species and the desorption states of hydrogen on the clean surface. Hydrogen initially adsorbs symmetrically in four-fold hollows (β_2); higher coverages lead to the conversion of hydrogen to asymmetric three-fold sites (β_1) within the hollow. At saturation coverages, both species coexist with the asymmetric moiety dominating. Vibrational spectra demonstrate the expected isotope shifts for deuterium solely due to differences in zero-point vibrational energies. Desorption from the asymmetric three-fold bound species demonstrates psuedo first-order kinetics with an activation energy of 14.1 kcal/mol. Desorption of the isotope shows no kinetic isotope effect. Coadsorption of CO into the four-fold hollows is blocked by the preadsorbed hydrogen, limiting adsorption to bridge and atop species; desorption and vibrational data indicate this hydrogen adatom is bound in a position of lower ligancy within the four-fold hollow. While the perturbed species exhibits a weakened Fe–H bond, the vibrational frequency is shifted nearly 200 cm^{-1} higher, representative of the new binding geometry. Site conversion of CO into the four-fold hollows occurs only upon initial desorption of H_2 from the surface. The demonstration that CO weakens the Fe–H bond upon coadsorption and alters the binding geometry is consistent with its role in promoting the novel hydrogen transfer reaction for adsorbed alkyl groups.

Acknowledgement

The authors gratefully acknowledge the support of the National Science Foundation (NSF CHE 89-19406-A1) without which this work would not have been possible.

References

[1] M.L. Burke and R.J. Madix, J. Am. Chem. Soc. 113 (1991) 1475.
[2] M.L. Burke and R.J. Madix, J. Am. Chem. Soc. 113 (1991) 4151.
[3] M.L. Burke and R.J. Madix, J. Am. Chem. Soc. 113 (1991) 3675.
[4] M.L. Burke and R.J. Madix, Surf. Sci. 237 (1990) 20.
[5] J.B. Benziger and R.J. Madix, Surf. Sci. 94 (1980) 119.
[6] D.W. Moon, S.L. Bernasek, J.-P. Lu, J.L. Gland and D.J. Dwyer, Surf. Sci. 184 (1987) 90.
[7] D.W. Moon, S.L. Bernasek, D.J. Dwyer and J.L. Gland, J. Am. Chem. Soc. 107 (1985) 4363.
[8] C. Benndorf, B. Kruger and F. Thieme, Surf. Sci. 163 (1985) L675.
[9] P.B. Merrill and R.J. Madix, Surf. Sci. 271 (1992) 81.
[10] J.B. Benziger and R.J. Madix, Surf. Sci. 115 (1982) 279.
[11] K. Christmann, Surf. Sci. Rep. 9 (1988) 1.
[12] A.M. Baro, H. Ibach and H.D. Bruchmann, Surf. Sci. 88 (1979) 384.
[13] H. Conrad, R. Scala, W. Stenzel and R. Unwin, J. Chem. Phys. 81 (1984) 6371.
[14] H. Conrad, M.E. Kordesch, R. Scala and W. Stenzel, J. Electron Spectrosc. Relat. Phenom. 38 (1986) 289.
[15] H. Conrad, M.E. Kordesch, W. Stenzel, M. Sunjic and B. Trminic-Radja, Surf. Sci. 178 (1986) 578.
[16] W. Ho, R.F. Willis and E.W. Plummer, Phys. Rev. Lett. 40 (1978) 1463.
[17] S.D. Cameron and D.J. Dwyer, Langmuir 4 (1988) 282.
[18] J.-P. Lu, M.R. Albert and S.L. Bernasek, Surf. Sci. 215 (1989) 348.
[19] W.-H. Hung, J. Schwartz and S.L. Bernasek, Surf. Sci. 248 (1991) 332.
[20] J.L. Falconer and R.J. Madix, J. Catal. 48 (1977) 262.
[21] J.L. Falconer and R.J. Madix, Surf. Sci. 48 (1975) 393.
[22] These results have a small error due to calculation of coverage for the β_1 state; with interference of the low temperature feature at 210 K, and uncertainty of defining the baseline between the β_1 and β_2 states, the coverage was underestimated by up to 10% in extreme cases. This error is expected to overestimate the reaction order and underestimate the activation energy. For purposes of an accurate determination of the activation energy of desorption, it appears that the heating rate variation for saturated adlayers would be more reliable given the desorption spectra. However, application of the isotherm–isostere analysis to this data does serve to demonstrate a few points.
[23] T.H. Lowry and K.S. Richardson, Mechanism and Theory in Organic Chemistry, 2nd ed. (Harper & Row, New York, 1981).
[24] U. Seip, M.-C. Tsai, K. Christmann, J. Kuppers and G. Ertl, Surf. Sci. 139 (1984) 29.
[25] L.R. Clavenna and L.D. Schmidt, Surf. Sci. 22 (1970) 365.
[26] A. Sellidj and J.L. Erskine, Surf. Sci. 220 (1989) 253.
[27] R.F. Willis, Surf. Sci. 89 (1979) 457.
[28] R.F. Willis, W. Ho and E.W. Plummer, Surf. Sci. 80 (1979) 593.
[29] It should be noted that the H/W(100) system differs

significantly from Fe(100) in that it exhibits reconstruction as a function of both temperature and θ_H. We have no evidence to suggest such a dynamic situation for Fe(100).

[30] C.M. Mate and G.A. Somorjai, Phys. Rev. B 34 (1986) 7417.

[31] F. Bozso, G. Ertl, M. Grunze and M. Weiss, Appl. Surf. Sci. 1 (1977) 103.

[32] Mode analysis of the EELS data can potentially provide great insight in the assignment of the species. For instance, with the C_{4v} atop and four-fold sites, one would expect to observe a single dipole mode in the specular direction, with a single doubly degenerate impact mode which would remain undetected. The C_{2v} bridge center would similarly possess a single dipole mode and two impact modes. A "quasi" three-fold site of C_s symmetry would conversely demonstrate two dipole modes, with a single impact mode. It must be noted however, that the data available is limited to specular EELS. Several studies have clearly demonstrated that without a systematic study of the energy and angle of incidence of the primary electron beam, dipole modes of hydrogen may remain unobserved in the specular direction [13,52]. For these reasons, our conclusions cannot be based upon the absence of modes.

[33] D.J. Dwyer, B. Rausenberger, J.-P. Lu et al., Surf. Sci. 224 (1989) 375.

[34] D.W. Moon, S.D. Cameron, F. Zaera et al., Surf. Sci. 180 (1987) L123.

[35] G. Blyholder, J. Head and F. Ruette, Surf. Sci. 131 (1983) 403.

[36] H. Ibach and D.L. Mills, Electron Energy Loss Spectroscopy and Surface Vibrations (Academic Press, New York, 1982).

[37] G.B. Blanchet, N.J. DiNardo and E.W. Plummer, Surf. Sci. 118 (1982) 496.

[38] N. Sheppard, Vibrational Spectroscopy of Adsorbates, Ed. R.F. Willis (Springer, Berlin, 1980) p. 165.

[39] J.A. Prybyla, P.J. Estrup and Y.J. Chabal, J. Vac. Sci. Technol. A 5 (1987) 791.

[40] J.A. Prybyla, P.J. Estrup and Y.J. Chabal, J. Chem. Phys. 94 (1991) 6274.

[41] W. Ho, N.J. DiNardo and E.W. Plummer, J. Vac. Sci. Technol. A 17 (1980) 134.

[42] M.A. Barteau, J.Q. Broughton and D. Menzel, Surf. Sci. 133 (1983) 443.

[43] C.M. Mate, B.E. Bent and G.A. Somorjai, Hydrogen Effects in Catalysis, Eds. Z. Paal and P.G. Menon (Marcel Dekker, New York, 1988) p. 57.

[44] A.M. Baro and W. Erley, Surf. Sci. 112 (1981) L759.

[45] W. Moritz, R. Imbihl, R.J. Behm, G. Ertl and T. Matsushima, J. Chem. Phys. 83 (1985) 1959.

[46] N.J. DiNardo and E.W. Plummer, Surf. Sci. 150 (1985) 89.

[47] M. Nishijima, S. Masuda, M. Jo and M. Onchi, J. Electron Spectrosc. Relat. Phenom. 29 (1983) 273.

[48] M. Nishijima, M. Jo and M. Onchi, Surf. Sci. 151 (1985) L179.

[49] M. Jo, M. Onchi and M. Nishijima, Surf. Sci. 154 (1985) 417.

[50] H. Ibach, S. Lehwald and B. Voigtlander, J. Electron Spectrosc. Relat. Phenom. 44 (1987) 263.

[51] K. Christmann, Mol. Phys. 66 (1989) 1.

[52] G. Lauth, E. Schwartz and K. Christmann, J. Chem. Phys. 91 (1989) 3729.

[53] S. Anderson, Chem. Phys. Lett. 55 (1978) 185.

[54] P.-A. Karlsson, A.-S. Martensson, S. Andersson and P. Nordlander, Surf. Sci. 175 (1986) L759.

[55] L.J. Richter and W. Ho, J. Vac. Sci. Technol. A 5 (1987) 453.

[56] C. Nyberg and C.G. Tengstal, Solid State Commun. 44 (1982) 251.

[57] C. Nyberg and C.G. Tengstal, Phys. Rev. Lett. 50 (1983) 1690.

[58] J.A. Prybyla and P.J. Estrup, Surf. Sci. 290 (1993) 413.

[59] K. Christmann, Z. Naturforsch. 34a (1979) 22.

[60] K. Christmann, O. Schober, G. Ertl and M. Neumann, J. Chem. Phys. 60 (1974) 4528.

[61] S. Johnson and R.J. Madix, Surf. Sci. 108 (1981) 77.

[62] K. Christmann, R.J. Behm, G. Ertl, M.A. Van Hove and W.H. Weinberg, J. Chem. Phys. 70 (1979) 4168.

[63] R.J. Behm, K. Christmann and G. Ertl, Surf. Sci. 99 (1980) 320.

[64] J.E. Huheey, Inorganic Chemistry, 3rd ed. (Harper & Row, New York, 1983) p. 258.